

Hadroproduction of t anti- t pair with a b anti- b pair using PowHel

A. Kardos¹ and Z. Trócsányi²

¹ INFN, Sezione di Milano-Bicocca, I 20126 Milano, Italy

² Institute of Physics and MTA-DE Particle Physics Research Group,
University of Debrecen, H-4010 Debrecen P.O.Box 105, Hungary

E-mail: Adam.Kardos@mib.infn.it, Z.Trocsanyi@atomki.mta.hu

Abstract. We simulate the hadroproduction of a $t\bar{t}$ pair in association with a $b\bar{b}$ pair at 14 TeV LHC using the PowHel package. We use the generated events, stored according to the Les-Houches event format, to make predictions for differential distributions formally at the next-to-leading order (NLO) accuracy and we compare these to existing predictions accurate at NLO.

PACS numbers: 12.38.-t, 14.65.Ha, 14.65.Fy

Submitted to: *J. Phys. G: Nucl. Phys.*

1. Introduction

According to the latest, most precise measurements, the t -quark mass is $m_t = 173.5 \pm 0.6 \pm 0.8$ GeV [1], indicating that the Yukawa coupling of the t -quark, $y_t = 0.997 \pm 0.008$ equals one with better than 1% accuracy. This remarkable result suggests that it is important to measure this coupling also directly as precisely as possible. After the recent discovery of a Higgs boson at the LHC [2, 3], the focus of analyses is shifting towards determining whether the couplings of this new particle to other fundamental particles agree with the Standard Model (SM) expectations. The measurement of the $t\bar{t}H$ coupling is important also because deviation from the SM expectation provides a signal of physics beyond the SM. The Higgs boson with mass approximately 125 GeV does not decay into a pair of t -quarks, therefore the only process to measure the $t\bar{t}H$ coupling in a model independent way is the study of hadroproduction of the Higgs-boson in association with a $t\bar{t}$ pair [4, 5].

The produced Higgs-boson decays immediately and only its decay products can be observed. According to the SM predictions, such a Higgs-boson decays dominantly into a $b\bar{b}$ pair. Thus one can plan to measure the $t\bar{t}H$ coupling in the $pp \rightarrow t\bar{t}H \rightarrow t\bar{t}b\bar{b}$ process. Unfortunately, this process has a large background from the direct QCD process $pp \rightarrow t\bar{t}b\bar{b}$. In order to make a proper background estimation and optimize the experimental selection of the $t\bar{t}H$ events, one needs simulation of the QCD background with high precision.

The most up to date method to simulate LHC processes with high precision is matching NLO QCD predictions to shower Monte Carlo programs (SMC). Presently, two formalisms are used frequently to match matrix element (ME) calculations at the NLO accuracy to parton showers (PS), the MC@NLO [6, 7] and POWHEG [8, 9] methods. Indeed, both methods were used to make predictions for $t\bar{t}H$ hadroproduction [10, 11], and the two predictions were found to be in agreement in Ref. [12]. Here we make one step further and describe our implementation of the $pp \rightarrow t\bar{t}b\bar{b}$ process within the *PowHel* framework.

The *PowHel* framework combines the *POWHEG-Box* [13], a flexible program implementing the POWHEG method, and the *HELAC-NLO* package [14]. The output of *PowHel* is simulated events stored according to the Les Houches accord [15] (LHE). Those events can be fed into any shower Monte Carlo (SMC) program for generating events with hadrons. Using the same framework we already provided LHE's for several processes at the LHC, namely to the production of a $t\bar{t}$ -pair in association with a hard object, such as a jet [16], a scalar boson [11], or a vector boson [17].

The scope of this article is to present the simulation of the $t\bar{t}b\bar{b}$ LHE's. The corresponding predictions at the NLO accuracy were first presented in Refs. [18, 19, 20]. The process under consideration represents an example of unprecedented complexity in *PowHel*, which raises some technical difficulties, worth of detailed description.

2. Method

We use the POWHEG formula (see Eq. (3.4) in Ref. [9]) to estimate the cross section from events with either unresolved or resolved first radiation,

$$d\sigma_{\text{LHE}} = \tilde{B}(\Phi_B) d\Phi_B \left[\Delta(\Phi_B, p_{\perp}^{\text{min}}) + d\Phi_{\text{rad}} \Delta(\Phi_B, k_{\perp}(\Phi_R)) \right. \\ \left. \times \frac{R(\Phi_R)}{B(\Phi_B)} \Theta(k_{\perp}(\Phi_R) - p_{\perp}^{\text{min}}) \right]. \quad (1)$$

In (1) $\tilde{B}(\Phi_B)$ denotes the NLO-corrected fully differential cross section belonging to the underlying Born configuration Φ_B (the integration over the momentum fractions is included implicitly),

$$\tilde{B}(\Phi_B) = B(\Phi_B) + \mathcal{V}(\Phi_B) + \int d\Phi_{\text{rad}} \mathcal{R}(\Phi_R) + \int \frac{dx}{x} \left[G_{\oplus}(\Phi_B) + G_{\ominus}(\Phi_B) \right], \quad (2)$$

and $\Delta(\Phi_B, p_{\perp})$ is the POWHEG Sudakov form factor that exponentiates the integral of the ratio of the real radiation $R(\Phi_R)$ and Born $B(\Phi_B)$ contributions over the radiation phase space,

$$\Delta(\Phi_B, p_{\perp}) = \exp \left\{ - \int d\Phi_{\text{rad}} \frac{R(\Phi_R)}{B(\Phi_B)} \Theta(k_{\perp}(\Phi_R) - p_{\perp}) \right\}. \quad (3)$$

In (2) \mathcal{R} denotes the difference of the real emission part and the subtraction terms, $\mathcal{R}(\Phi_R) = R(\Phi_{n+1}) - C(\Phi_{n+1})$. Similarly, \mathcal{V} denotes the regularized (finite in $d = 4$ dimensions) virtual correction (was $V(\Phi_n)$ in Eq. (3.2) in Ref. [9]), i.e., it also contains the integrated subtraction terms, while we use $V(\Phi_n)$ to denote the unregularized virtual correction. Using $\tilde{B}(\Phi_B)$, we obtain the cross section at NLO accuracy as an integral over the Born phase space,

$$\sigma_{\text{NLO}} = \int d\Phi_B \tilde{B}(\Phi_B), \quad (4)$$

We used the `HELAC-NLO` package to generate the crossing symmetric matrix elements required in the `POWHEG-Box` as input. In particular, (i) the squared matrix elements for the flavour structures of the Born ($gg \rightarrow t\bar{t} b\bar{b}$, $q\bar{q} \rightarrow t\bar{t} b\bar{b}$, $\bar{q}q \rightarrow t\bar{t} b\bar{b}$) and real radiation emission ($q\bar{q} \rightarrow t\bar{t} b\bar{b}g$, $gg \rightarrow t\bar{t} b\bar{b}g$, $\bar{q}q \rightarrow t\bar{t} b\bar{b}q$, $g\bar{q} \rightarrow t\bar{t} b\bar{b}q$, $q\bar{q} \rightarrow t\bar{t} b\bar{b}g$, $qg \rightarrow t\bar{t} b\bar{b}q$, $gq \rightarrow t\bar{t} b\bar{b}q$) subprocesses ($q \in \{u, d, c, s\}$ – we neglect the contribution of b -quarks in the initial state), (ii) the colour-correlated and spin-correlated squared matrix elements for the Born flavour structures, and (iii) the finite part of the virtual correction contributions in dimensional regularization, on the basis of the OPP method [21] complemented by Feynman rules for the computation of the QCD R_2 rational terms [22]. With this input `POWHEG-Box` generates events with either unresolved or resolved first radiation. Then, one can use any shower Monte Carlo (SMC) program for generating events with hadrons.

2.1. Predictions at NLO accuracy

The process presented here was studied at the NLO accuracy in the literature [19, 20], which enabled us to make detailed checks of our calculation. We reproduced all figures of Ref. [19] and found complete agreement.

As this process has different hard scales in the final state the proper choice of the scale is important as the convergence of the perturbation series is influenced by that. For instance, with the central scale $\mu_R = \mu_F = \mu_0 = m_t$, the NLO correction is large, about 80% [19]. It was pointed out in Ref. [20] that the convergence is much better with the central scale $\mu_0^2 = m_t \sqrt{p_{\perp,b} p_{\perp,\bar{b}}}$, when NLO corrections amount to about 24%. This scale was inspired by scale choices made in shower Monte Carlo programs and is designed to mimic the effect of higher order corrections in the low-order prediction. It is close to the scale where the scale dependence at NLO accuracy reaches its maximum, leaving little room for positive higher order corrections: the predictions with the central scale appear near the higher edge of the scale-dependence bands.

As our goal is to generate the effect of higher-order corrections by the shower, in generating pre-showered events ready for feeding those into SMC's, we find more appropriate to use the central scale $\mu_0 = H_{\perp}/2$, where H_{\perp} is the sum of transverse masses $m_{\perp,f} = \sqrt{m_f^2 + p_{\perp,f}^2}$ of the final-state partons in the hard-scattering event, $H_{\perp} = \sum_f m_{\perp,f}$ (the sum includes four partons at LO and in the virtual correction, while five partons in the real correction). This choice reproduces better the standard choice for the $t\bar{t}$ final state near threshold production of the final state: as $p_{\perp,b}$ and $p_{\perp,\bar{b}} \rightarrow 0$, $\mu_0 \rightarrow m_{\perp,t}$. In Figure 1 we show our predictions for the total cross section with the following selection cuts (setup I in Ref. [20]):

- (i) A massless parton was considered as a possible jet constituent if its pseudorapidity is within the range $[-5, +5]$ ($|\eta| < 5$).
- (ii) Jets were reconstructed with the k_{\perp} -algorithm using $p_{\perp,\text{jet}}^{\text{min}} = 20$ GeV and $R = 0.4$.
- (iii) We required at least one b - and one \bar{b} -jet, with $|y_{b(\bar{b})}| < 2.5$. (We distinguish between quark flavours and tagged jets using roman typesetting for the former and italic for the latter.)
- (iv) Events with invariant mass of the $b\bar{b}$ -jet pair below $m_{b\bar{b}}^{\text{min}} = 100$ GeV were discarded.

Clearly, our choice for the default scale gives as stable predictions at NLO as those with $\mu_0^2 = m_t \sqrt{p_{\perp,b} p_{\perp,\bar{b}}}$. The cross section with this default scale is 534 fb at LO and 630 fb at NLO, so the NLO K-factor is 1.18, and the NLO scale-uncertainty in the range $[\mu_0/2, 2\mu_0]$ is ${}^{+22}_{-32}\%$. The shapes of the distributions are very similar at LO and NLO accuracies as seen in Figures 2 and 3. In the same figures we also show the bands representing the scale dependence due to the variation of the scale in the range $[\mu_0/2, 2\mu_0]$. We find that the histograms with the default scale run in the middle of the band representing the scale dependence.

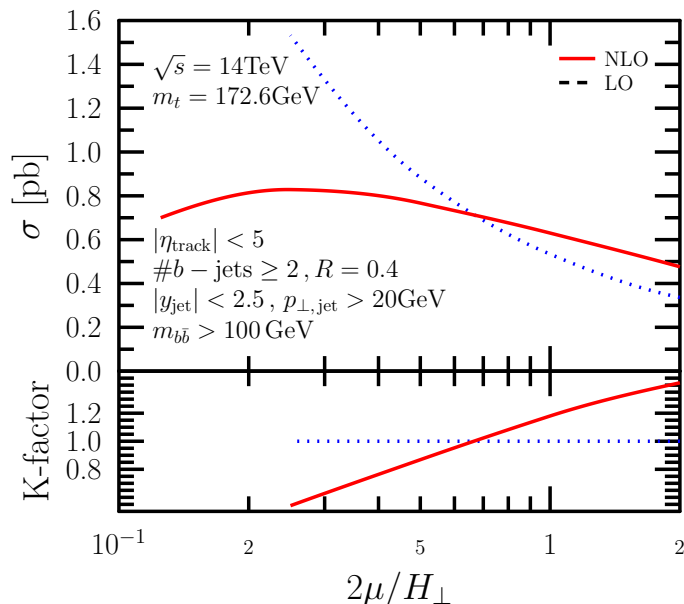


Figure 1. Dependence of the total cross section at LO and NLO accuracy, with cuts shown in the legend.

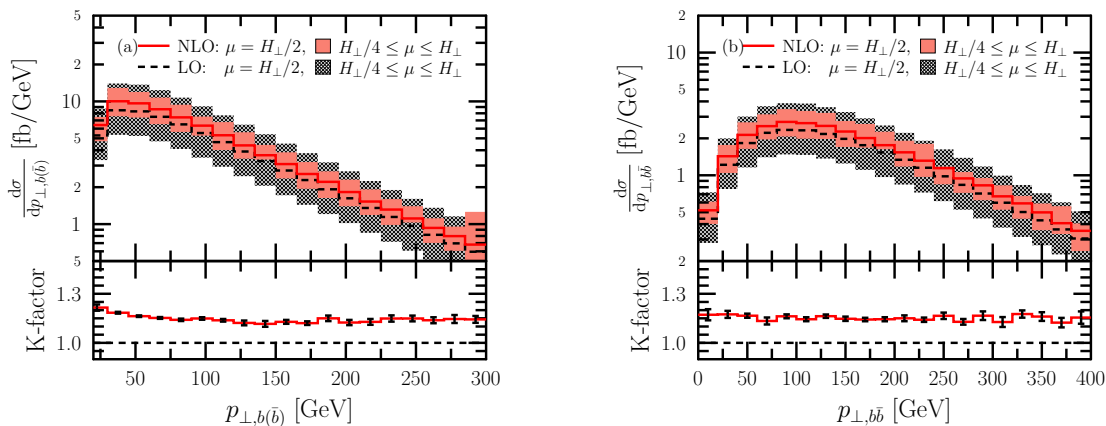


Figure 2. (a) Transverse momentum distribution of the b -jet and (b) that of the $b\bar{b}$ -jet pair at the LHC at $\sqrt{s} = 14$ TeV using PowHel1. The shaded bands correspond to cross sections obtained with varying the scale around the default one in the range $[\mu_0/2, 2\mu_0]$. The lower panels show the NLO predictions normalized by the predictions at LO, with errorbars representing the statistical accuracy of the numerical integration.

2.2. Generation cuts and suppression

As we treat the b -quarks massless, the fully differential Born cross section becomes singular if any of the transverse momenta of the b -quarks $p_{\perp,b}$ or $p_{\perp,\bar{b}}$, or the invariant mass of the $b\bar{b}$ -pair $m_{b\bar{b}}$ vanishes. To make the integral of B finite over the whole Born phase space, we introduce generation cuts by requiring $p_{\perp,b} \geq p_{\perp}^{(\text{g.c.})}$ and $m_{b\bar{b}} \geq m_{b\bar{b}}^{(\text{g.c.})}$, where $p_{\perp}^{(\text{g.c.})} = m_{b\bar{b}}^{(\text{g.c.})} = 2$ GeV. We checked that these generation cuts are sufficiently

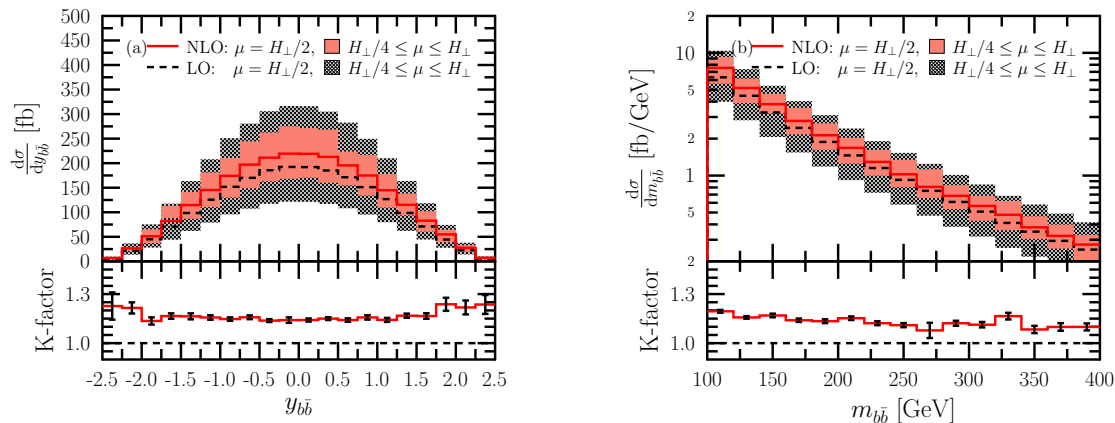


Figure 3. Same as Figure 2 for (a) the rapidity distribution and (b) invariant mass distribution of the $b\bar{b}$ -jet pair.

low, so that the physical predictions are independent of those when selection cuts characteristic to physical analyses are superimposed. However, with such low generation cuts the event generation is very inefficient because most of the events are generated in regions of the phase space where B is large, but those regions are usually not selected in the analyses. Therefore, we also introduce a suppression factor [23] for \tilde{B} of the form

$$\mathcal{F}_{\text{supp}} = \left(\frac{m_{b\bar{b}}^2}{m_{b\bar{b}}^2 + (m_{b\bar{b}}^{\text{supp}})^2} \right)^3 \prod_{i=b,\bar{b}} \left(\frac{p_{\perp,i}^2}{p_{\perp,i}^2 + (p_{\perp}^{\text{supp}})^2} \right)^3, \quad (5)$$

where $p_{\perp}^{(\text{supp})} = m_{b\bar{b}}^{(\text{supp})} = 30$ GeV. Such a suppression factor does not influence physical observables, which we checked explicitly.

2.3. Precision and efficient evaluation of loop amplitudes

For this process there is the high degree of difficulty of evaluating the loop amplitudes. The high-rank of the tensor loop-integrals makes the numerical computation of the loop amplitude unstable, and thus, unreliable when double precision arithmetics is used in `CutTools` [24], as implemented in `HELAC-1loop` (part of `HELAC-NLO`). In order to control numerical instabilities we employ an $\mathcal{N} = \mathcal{N}$ test as implemented in `CutTools`. This means that for a given numerator we determine the scalar-integral coefficients using double precision arithmetics. We check the accuracy of the integrand by reconstructing it using all the coefficients (and spurious terms) with a randomly chosen loop momentum. If the reached relative accuracy is worse than 10^{-4} , we pass the same phase space point in double-double precision (computed simultaneously with the double-precision version) to `HELAC-1loop@dd` to recalculate all the coefficients (using the multiple precision part of `CutTools`). The `HELAC-1loop@dd` code is a straightforward extension of `HELAC-1loop` to double-double precision using the package `QD` [25]. This way we solved all numerical instabilities in the computation of the virtual correction. The above procedure however,

makes the numerical computation of the loop amplitudes rather cumbersome, requiring much more CPU time. This problem is magnified by the hit-and-miss procedure, the way event generation is performed in the POWHEG-Box. During NLO integration the inclusive NLO cross section is computed simultaneously with the maximal value of \tilde{B}

$$\tilde{B}_{\max} = \max_{\Phi_B} \tilde{B}(\Phi_B). \quad (6)$$

When the underlying Born kinematics Φ_B is generated for an event, it is accepted if $\tilde{B}(\Phi_B) \geq \xi \tilde{B}_{\max}$, where ξ is a random number picked between zero and one. Using this hit-and-miss method, the \tilde{B} function has to be evaluated several times to find a suitable phase space point which is selected. If \tilde{B} is calculated multiple times per event, event generation becomes highly inefficient because \tilde{B} contains the virtual part, whose evaluation is very time consuming. To improve the efficiency, we first generate events with a fake virtual contribution, proportional to the Born cross section, $V = \alpha B$. The value of α is arbitrary. We select those events that pass the selection cuts, whose weights in a final step are reweighted by the true virtual contribution. In practice, we choose α such that the physical cross section changes only little with this reweighting. We have not made a systematic study to minimize the effect of reweighting, but chose $\alpha = 1/2$ after some simple test runs. Using the fake virtual, we can reduce the computation of the virtual contributions to few hundred thousand phase space points. The plots shown in the next section are based upon about 100 k LHE's.

The POWHEG method produces unweighted events. When we generate events with the fake virtual part, unweighting must be done using the NLO cross section obtained also with the fake virtual. After the events that pass the selection cuts are collected, we reweight those

$$\mathcal{W}|_{V=B/2} \rightarrow \mathcal{W} = \mathcal{W}|_{V=B/2} \frac{\tilde{B}(\Phi_B)}{\tilde{B}|_{V=B/2}(\Phi_B)}, \quad (7)$$

where $\mathcal{W}|_{V=B/2}$ is the weight with fake virtual, and \mathcal{W} is the weight with the true virtual part. Clearly, the new weight becomes dependent upon the underlying Born kinematics.

The majority of events generated by the POWHEG-Box have either positive or negative, but in magnitude equal weights. As seen on Figure 4, the relative fraction of the negative weights is at the percent level. (Due to the suppression in (5) there are also several large weight events starting at about 50 in Figure 4.) The drawback of the reweighting procedure is the appearance of many different weights, leaving only about 90 % of the events with equal positive weight.

3. Predictions from the LHE's

Using PowHel one can make predictions at four different stages in the evolution of the final state: (i) at the parton level using NLO accuracy, (ii) from the pre-showered POWHEG simulation (referred to as LHE's), formally at the NLO accuracy, (iii) after decay of the heavy particles, (iv) at the hadron level after full SMC. While in an

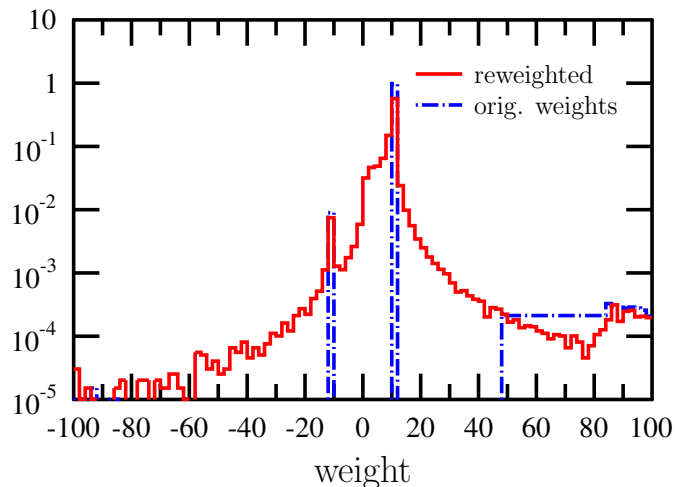


Figure 4. Distribution of weights before and after reweighting.

experimental analysis the last option is the most useful, for examining the effect of the different stages in the evolution, and also for checking purposes, it is useful to study the predictions at intermediate stages. In the previous section we mentioned that we made comparisons with existing predictions at stage (i) and found agreement. We now show predictions at stage (ii), together with the dependence on the choice of the scale μ_0 , and leave the phenomenological analyses at the remaining stages to a more detailed publication.

Our selection cuts are the same as in the NLO study above (setup 1 of Ref. [20]). In Figures 5 and 6 we show our predictions for kinematic distributions of the leading and second hardest b -jet, respectively while in Figures 7 and 8 we present our predictions for those of the b -jet pair: transverse momentum and rapidity in Figure 7, separation of the b -jets in rapidity–azimuthal angle plane ($\Delta R_{b\bar{b}} = \sqrt{\Delta y_{b\bar{b}}^2 + \Delta \phi_{b\bar{b}}^2}$) and their invariant mass in Figure 8. The two bands correspond to predictions obtained by varying the equal renormalization and factorization scales in the range $[\mu_0/2, 2\mu_0]$ around the fixed default scale $\mu_0 = H_\perp/2$. If the renormalization and factorization scales are varied independently in the same range, the scale uncertainty is smaller.

The distributions from the LHE’s have the same shape as those at NLO accuracy, but the normalization is larger by about 20%. The two predictions agree within the scale uncertainty of the NLO prediction, which is the formal accuracy of the POWHEG method. Thus these LHE’s can be fed into SMC’s for generating events at hadron level and perform experimental analyses.

4. Conclusions

We have implemented the hadroproduction of a $t\bar{t}$ -pair in association with a $b\bar{b}$ -pair, $pp \rightarrow t\bar{t}b\bar{b}$, in the PowHel framework, which can be used to generate LHE files.

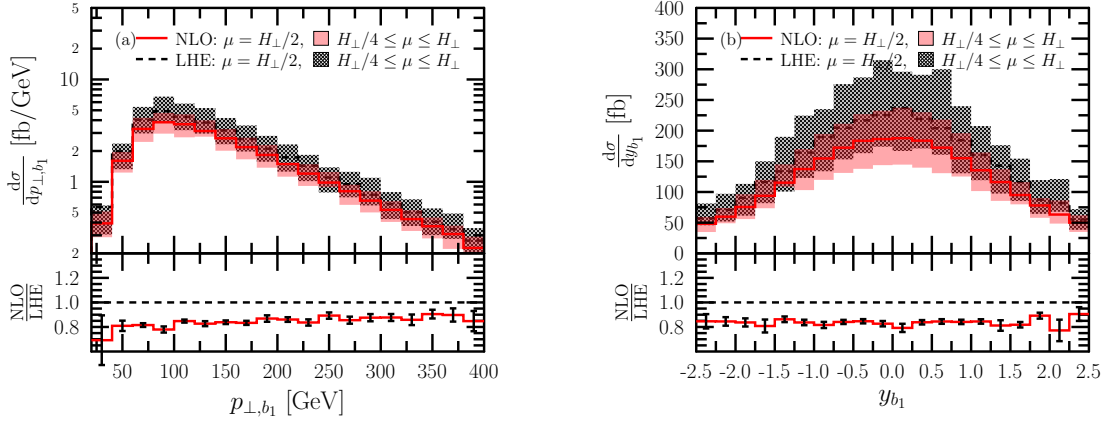


Figure 5. Distribution of (a) transverse momentum (b) rapidity of the hardest b -jet at the LHC at $\sqrt{s} = 14$ TeV using PowHel1. Distributions from LHE's are denoted LHE, while those at NLO accuracy by NLO. The shaded bands correspond to cross sections obtained with varying the scale around the default one in the range $[\mu_0/2, 2\mu_0]$. The lower panels show the NLO predictions normalized by the predictions from LHE's, with errorbars representing the combined statistical accuracy of the numerical integrations.

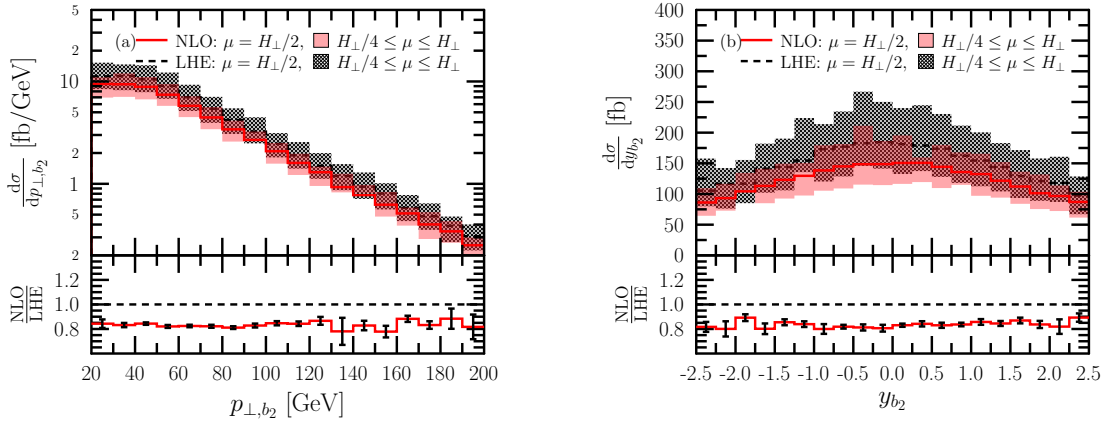


Figure 6. Same as Figure 5 for the second hardest b -jet.

We discussed the technical subtleties of such event simulations, in particular, issues related to the efficient generation of the events for such a complex process: (i) the choice of renormalization and factorization scales for generating the LHE's, (ii) the implementation of higher precision arithmetics in computing the loop amplitudes with sufficient precision, (iii) the advantage of performing the event generation with fake virtual part and the method of reweighting.

The event files produced by PowHel1, together with further detail and results of our project, the corresponding version of the program are available at <http://grid.kfki.hu/twiki/bin/view/DbTheory>. We are confident that these LHE's are suitable input into SMC's to produce distributions at the hadron level needed for experimental analyses. Thus using those events one can make a detailed analysis of $t\bar{t}H$ signal and $t\bar{t}b\bar{b}$ background predictions at the hadron level.

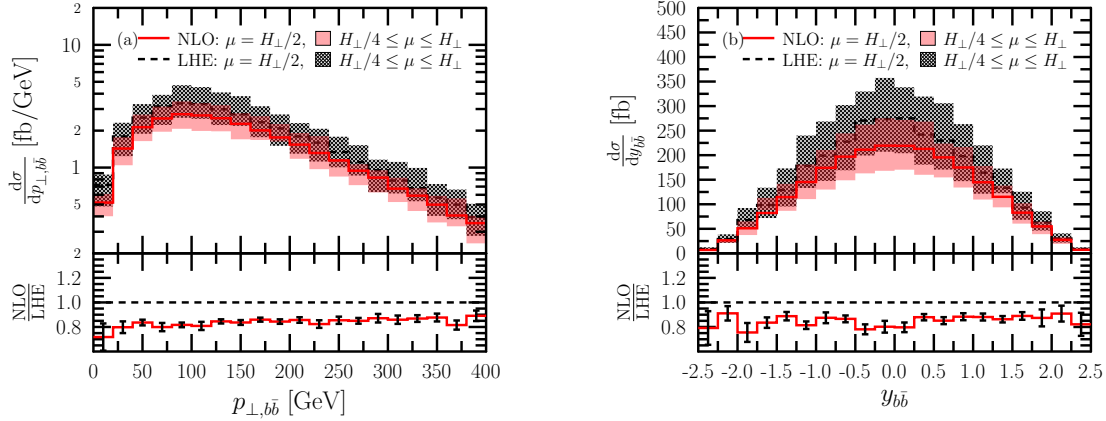


Figure 7. Same as Figure 5 for the distribution of (a) transverse momentum and (b) rapidity of the $b\bar{b}$ -jet pair.

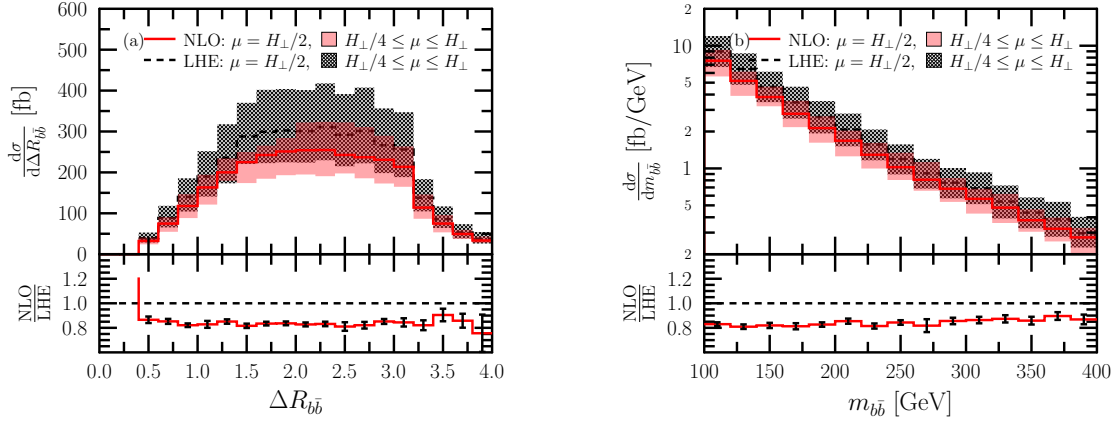


Figure 8. Same as Figure 5 for the distribution of (a) $\Delta R_{b\bar{b}}$ separation and (b) invariant mass of the $b\bar{b}$ -jet pair.

Acknowledgments

We are grateful to M.V. Garzelli, A. van Hameren, P. Nason and M. Worek for useful discussions. This research was supported by the Hungarian Scientific Research Fund grant K-101482, the European Union and the European Social Fund through LHCPHenoNet network PITN-GA-2010-264564, and the Supercomputer, the national virtual lab TAMOP-4.2.2.C-11/1/KONV-2012-0010 project.

References

- [1] Beringer J *et al.* (Particle Data Group) 2012 *Phys.Rev.* **D86** 010001
- [2] Aad G *et al.* (ATLAS Collaboration) 2012 *Phys.Lett.* **B710** 49–66 (*Preprint 1202.1408*)
- [3] Chatrchyan S *et al.* (CMS Collaboration) 2012 *Phys.Lett.* **B710** 26–48 (*Preprint 1202.1488*)
- [4] Maltoni F, Rainwater D L and Willenbrock S 2002 *Phys.Rev.* **D66** 034022 (*Preprint hep-ph/0202205*)
- [5] Belyaev A and Reina L 2002 *JHEP* **0208** 041 (*Preprint hep-ph/0205270*)
- [6] Frixione S and Webber B R 2002 *JHEP* **06** 029 (*Preprint hep-ph/0204244*)

- [7] Frixione S, Stoeckli F, Torrielli P, Webber B R and White C D 2010 *arXiv:1010.0819[hep-ph]* (Preprint 1010.0819)
- [8] Nason P 2004 *JHEP* **11** 040 (Preprint hep-ph/0409146)
- [9] Frixione S, Nason P and Oleari C 2007 *JHEP* **11** 070 (Preprint 0709.2092)
- [10] Frederix R *et al.* 2011 *Phys. Lett.* **B701** 427–433 (Preprint 1104.5613)
- [11] Garzelli M, Kardos A, Papadopoulos C and Trocsanyi Z 2011 *Europhys.Lett.* **96** 11001 (Preprint 1108.0387)
- [12] Dittmaier S, Mariotti C, Passarino G, Tanaka R *et al.* 2012 (Preprint 1201.3084)
- [13] Alioli S, Nason P, Oleari C and Re E 2010 *JHEP* **06** 043 (Preprint 1002.2581)
- [14] Bevilacqua G, Czakon M, Garzelli M, van Hameren A, Kardos A *et al.* 2013 *Comput.Phys.Commun.* **184** 986–997 (Preprint 1110.1499)
- [15] Alwall J *et al.* 2007 *Comput. Phys. Commun.* **176** 300–304 (Preprint hep-ph/0609017)
- [16] Kardos A, Papadopoulos C and Trocsanyi Z 2011 *Phys.Lett.* **B705** 76–81 (Preprint 1101.2672)
- [17] Garzelli M, Kardos A, Papadopoulos C and Trocsanyi Z 2012 *JHEP* **1211** 056 (Preprint 1208.2665)
- [18] Bredenstein A, Denner A, Dittmaier S and Pozzorini S 2009 *Phys.Rev.Lett.* **103** 012002 (Preprint 0905.0110)
- [19] Bevilacqua G, Czakon M, Papadopoulos C, Pittau R and Worek M 2009 *JHEP* **0909** 109 (Preprint 0907.4723)
- [20] Bredenstein A, Denner A, Dittmaier S and Pozzorini S 2010 *JHEP* **1003** 021 (Preprint 1001.4006)
- [21] Ossola G, Papadopoulos C G and Pittau R 2007 *Nucl. Phys.* **B763** 147–169 (Preprint hep-ph/0609007)
- [22] Draggiotis P, Garzelli M V, Papadopoulos C G and Pittau R 2009 *JHEP* **04** 072 (Preprint 0903.0356)
- [23] Alioli S, Nason P, Oleari C and Re E 2011 *JHEP* **1101** 095 (Preprint 1009.5594)
- [24] Ossola G, Papadopoulos C G and Pittau R 2008 *JHEP* **0803** 042 (Preprint 0711.3596)
- [25] Hida Y, Li X S and Bailey D H 2000 Quad-double arithmetic: Algorithms, implementation, and application Tech. Rep. LBNL-46996 Lawrence Berkeley National Laboratory Berkeley, CA 94720 available at <http://www.nersc.gov/~dhbailey/mpdist/mpdist.html>